



Cite this: *Soft Matter*, 2026, 22, 2880

Symmetry breaking of interacting charge-regulated planar macroions at low salt concentration

Ahmad M. N. Itani, ^a Guilherme Volpe Bossa, ^b Faruk Hossain ^a and Sylvio May ^{*a}

The charge of macroions such as colloids and membranes can often be regulated by reversible ion adsorption or dissociation reactions. When two chemically identical macroions interact across an electrolyte, charge regulation will typically lead to the same charge density on both macroion surfaces. However, it was recently demonstrated that a non-ideal, Frumkin-like adsorption behavior of the ions can lead to a spontaneous symmetry breaking, where the coupling of charge regulation leads to different surface charge densities on both macroions in thermal equilibrium. While previous modeling was carried out numerically in the presence of salt for selected systems, we argue that the no-salt limit captures experimentally relevant situations at low salt concentration. We therefore focus on macroions with dissociable surface groups in the absence of salt, where the Poisson–Boltzmann equation can be solved analytically and the spontaneous emergence of uniform but different degrees of dissociation on both macroions signifies a symmetry breaking. Using a perturbation approach we derive analytic results for the local stability of the symmetric state. This not only provides a complete thermodynamic characterization of the symmetry breaking as function of all parameters, it also uncovers previously unrecognized features. First, depending on the degree of non-ideality, the symmetry breaking transition can be continuous or discontinuous. Second, metastable states do exist far away from critical points but not in their vicinity. And third, electrostatic interactions generally act toward weakening or suppressing the occurrence of symmetry breaking.

Received 6th March 2026,
Accepted 23rd March 2026

DOI: 10.1039/d6sm00194g

rsc.li/soft-matter-journal

1 Introduction

Experimental studies suggest the complex surface chemistry of colloidal particles¹ can alter mutual interactions² and even trigger self-assembly *via* long-range forces, especially under low salt conditions.^{3–5} Electrostatic modeling through Poisson–Boltzmann theory generally predicts repulsion between identical macroions,⁶ but when adjusting solvation properties^{1,7} or charge regulation^{2,8,9} at the surfaces of the involved macroions introduce additional order parameters, unexpected new properties can emerge even on the level of mean-field theory,^{10,11} including non-monotonic screening lengths, buffering of the background electrolyte, and the possibility of long-range attraction between nominally like-charged objects. Not surprisingly, there has been considerable interest in modeling interacting macroions that are

subject to a charge regulation mechanism using continuum electrostatics and computer simulations.^{12–18}

Charge regulation, the adjustment of a surface's effective charge through reversible association and dissociation of ions,¹⁹ is based on an underlying adsorption isotherm. Of particular interest is charge regulation through Frumkin-type adsorption,²⁰ which goes beyond the Langmuir adsorption model of independent adsorption sites by accounting for lateral interactions between already adsorbed ions. The Frumkin isotherm, also referred to as Frumkin–Fowler–Guggenheim isotherm, is frequently used to model the adsorption of contaminants such as heavy metals, dyes, and organics on porous carbons, clays, and oxides^{21–24} but also for the adsorption of ionic surfactants and other amphiphiles on fluid interfaces,^{25–28} the adsorption of hydrogen on platinum nanoparticles,²⁹ or the intercalation of lithium into inorganic host materials.³⁰ The nature and magnitude of lateral interactions among adsorbents has been estimated based on Frumkin-type adsorption isotherms for a multitude of systems such as the adsorption of surfactin on the liquid–air interface,³¹ ion-exchange and charge-regulation phenomena at surfaces of

^a Department of Physics, North Dakota State University, Fargo, ND 58108, USA.
E-mail: sylvio.may@ndsu.edu

^b Institute of Mathematical and Physical Sciences, Universidad Austral de Chile, Valdivia 5090000, Chile



metal oxide particles immersed in aqueous electrolyte solutions,³² and the competitive adsorption of ions on mineral surfaces.³³

In a series of studies, Podgornik and coworkers^{34–37} have proposed the occurrence of a spontaneous symmetry breaking for interacting, charge-regulated surfaces of chemically identical macroions. The symmetry breaking is driven by an underlying Frumkin–Fowler–Guggenheim isotherm that favors high and low effective charge densities over intermediate ones. Models for both planar³⁴ and spherical³⁷ macroions were analyzed in the presence of monovalent salt, and numerical solutions of the Poisson–Boltzmann equation were used to predict when symmetry breaking occurs. Simple analytic solutions of interacting macroions are, in general, not available in the presence of salt. This makes the complete characterization of the symmetry breaking as function of all parameters challenging. However, we argue that experimental studies of interacting, charge-regulated macroions such as colloidal particles or charged lipid membranes are often carried out at sufficiently low salt concentrations, at which the presence of salt can be ignored altogether and interacting macroions can be modeled under no-salt conditions. For monovalent salt, this is the case when the Debye screening length $l_D \gg a/l_B$ is much larger than the ratio of average cross-sectional area per charge a divided by the Bjerrum length l_B . The advantage of the no-salt regime is the availability of simple analytic solutions of the non-linear Poisson–Boltzmann equation for interacting planar surfaces. The opportunity to completely and accurately characterize the stability of a highly nonlinear system that previously was amenable only to numerical analysis has motivated the present study.

In this work, we model the interaction between planar charge-regulated macroions in the absence of salt, where the Poisson–Boltzmann equation offers an analytic solution. As in preceding models by Podgornik and coworkers,^{10,34,37} we consider a charge regulation mechanism based on the Frumkin–Fowler–Guggenheim isotherm, which is equivalent to the mean-field Bragg–Williams free energy³⁸ in the way to account for non-electrostatic interactions between adsorbed ions. In contrast to the preceding studies, we assume surface groups become charged upon dissociation without the presence of additional adsorption sites for the counterions. Solutions of the Poisson–Boltzmann equation entail boundary conditions in the form of non-linear algebraic relationships. Using a perturbation approach we carry out a stability analysis, from which we obtain analytic predictions for the appearance of symmetry breaking. We demonstrate that broken symmetry exists only for intermediate distances between the macroions, but not for sufficiently small or large distances. In addition, we predict the existence of metastable symmetric states and present a stability diagram that fully describes the thermodynamic behavior of our model as function of all parameters. Finally, we discuss the applicability of the no-salt assumption to experimental situations, assess the role of electrostatic interactions for the appearance of spontaneous symmetry breaking, characterize the stability limit of an isolated macroion, and calculate the disjoining pressure between the two macroions.

2 Theory

We represent two interacting macroions by two very large planar and parallel surfaces of lateral area A , indexed “1” and “2” and separated by a distance d . Each macroion carries a fixed bare surface charge density $\sigma = -e/a$ of negative sign, where a denotes the average cross-sectional area per elementary charge e . The net surface charge density of the macroion is equal to σ only when all counterions are released and none is located at the macroion surface. Sandwiched between the two planar macroions is an electrolyte that contains counterions only. The total number of counterions is $N = 2A/a$. Allowing for charge regulation, we assume counterions can be associated with or dissociated from the macroion surfaces. If $N_1 = \phi_1 A/a$ and $N_2 = \phi_2 A/a$ counterions are associated with macroions “1” and “2”, respectively, the remaining $N_f = N - N_1 - N_2$ counterions are mobile, thus forming a diffuse counterion cloud between the two surfaces. Counterion association reduces the net surface charge densities from σ to the effective values $\sigma_1 = -(1 - \phi_1)e/a$ and $\sigma_2 = -(1 - \phi_2)e/a$, where ϕ_1 and ϕ_2 describe the degree of counterion association on each macroion, with $0 \leq \phi_1 \leq 1$ and $0 \leq \phi_2 \leq 1$. If $\phi_1 = \phi_2 = 0$, all counterions reside in the electrolyte and $\sigma_1 = \sigma_2 = \sigma$ has the largest possible magnitude. If $\phi_1 = \phi_2 = 1$, all counterions are associated with the two macroions and $\sigma_1 = \sigma_2 = 0$ vanishes. Fig. 1 shows a schematic representation of the two planar macroions, with some counterions being macroion-associated and the remaining ones dissociated, forming a diffuse cloud of mobile counterions.

When the distance d between the planar macroions changes, ϕ_1 and ϕ_2 , as well as the local concentration of the intervening mobile counterions (denoted below by n), can adjust.

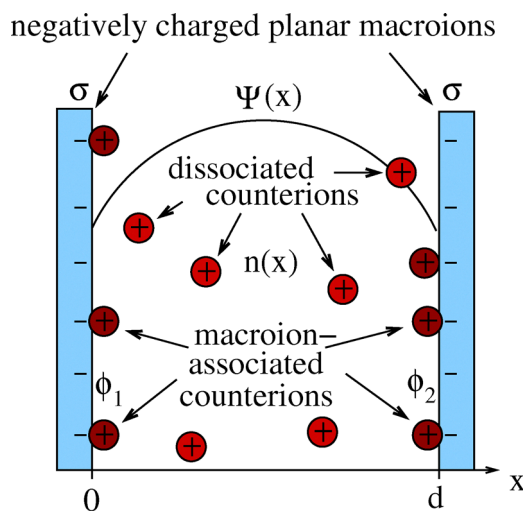


Fig. 1 Two planar macroions (shown in blue) carry a bare surface charge density σ , with counterions either associated with the surfaces (shown in dark red) or dissociated and thus being mobile in solution between the two macroions (shown in red). No salt is added. The macroion surfaces are located at positions $x = 0$ and $x = d$, with the x -coordinate pointing normal to the surfaces. The fractions ϕ_1 and ϕ_2 characterize the degrees of counterion association on macroions “1” and “2”, respectively. The local concentration of the intervening mobile counterions is denoted by $n(x)$, and the dimensionless electrostatic potential $\Psi(x)$ is shown schematically.



Characterization of this adjustment is the goal of the present work. We point out an important assumption: while the degrees of counterion association ϕ_1 and ϕ_2 can be different on each macroion, they are assumed to be uniform along each individual macroion surface. At least for isolated macroions we will make sure in this work that the degrees of counterion association remain uniform. For interacting macroions, however, the uniformity stands as an assumption.

We assume counterion association with a macroion surface is driven by a fixed association energy λ per counterion. In this work, all energies are expressed in units of the thermal energy $k_B T$, Boltzmann constant times absolute temperature. Hence, λ is a dimensionless quantity. We also consider a non-ideal contribution to the counterion association/dissociation isotherm and describe this by using the Bragg–Williams free energy³⁸ per charged site on each macroion surface,

$$f_{\text{BW}}(\phi) = \phi \ln \phi + (1 - \phi) \ln(1 - \phi) + \chi \phi(1 - \phi), \quad (1)$$

where χ is a non-ideality parameter. Positive χ amounts to an effective non-electrostatic attraction between surface-associated counterions. The present work studies the consequences of $\chi > 0$ without investigating the molecular origin that could give rise to attractive interactions.¹ We note that our counterion association/dissociation model based on the fixed association energy λ per counterion together with the non-ideality parameter χ in eqn (1) is equivalent to the Frumkin–Fowler–Guggenheim isotherm²⁸ as it was used in preceding work.^{34,37} For $\chi = 0$, counterion association/dissociation follows the simple Langmuir adsorption model of an electrified surface.

We express the total free energy of the two macroions with their counterions either being macroion-associated or dissociated and thus residing in the electrolyte as

$$F = \frac{A}{a} [f_{\text{BW}}(\phi_1) + f_{\text{BW}}(\phi_2) - \lambda(\phi_1 + \phi_2)] + A \int_0^d dx \left[\frac{\Psi'^2}{8\pi l_B} + n \ln(n\nu) - n \right]. \quad (2)$$

The first line describes the non-ideal mixing free energies of the macroion-associated counterions together with their association energies. This involves the two parameters χ and λ . The second line expresses the free energy of the electrolyte, which occupies the space along the x -axis of a Cartesian coordinate system from the surface of macroion “1” (located at $x = 0$) to macroion “2” (located at $x = d$). All properties of our mean-field model depend only on the x -coordinate, including the dimensionless electrostatic potential $\Psi = \Psi(x)$ and the local counterion concentration $n = n(x)$. The term $\Psi'^2/8\pi l_B$ in the integrand characterizes the volume density of the electrostatic energy and l_B the Bjerrum length, thereby assuming a uniform dielectric constant in the solvent space between the macroions. Note that a prime denotes the derivative with respect to the argument; *i.e.* $\Psi' = d\Psi/dx$. The term $n \ln(n\nu) - n$ accounts for the local free energy density of an ideal gas, where the “thermal” volume ν depends only on the temperature T . Keeping T fixed renders ν a

constant. If we define the average counterion density in the electrolyte by $\bar{n} = (1/d) \times \int_0^d dx n$, the conservation constraint of the total number of counterions, $\phi_1 + \phi_2 + ad\bar{n} = 2$, can be incorporated into the free energy by defining

$$\tilde{F} = F - \Lambda \frac{A}{a} [ad\bar{n} - (1 - \phi_1) - (1 - \phi_2)], \quad (3)$$

where Λ is a Lagrangian multiplier. Accounting for Poisson's equation $\Psi'' = -4\pi l_B n$ allows us to calculate the first variation of \tilde{F} with respect to ϕ_1 , ϕ_2 , and n ,

$$\begin{aligned} \delta \tilde{F} = & \frac{A}{a} \delta \phi_1 [f'_{\text{BW}}(\phi_1) - \lambda + \Lambda + \Psi(0)] \\ & + \frac{A}{a} \delta \phi_2 [f'_{\text{BW}}(\phi_2) - \lambda + \Lambda + \Psi(d)] \\ & + A \int_0^d dx \delta n [\Psi + \ln(n\nu) + \Lambda]. \end{aligned} \quad (4)$$

Stationarity demands $\delta \tilde{F} = 0$. The variations $\delta \phi_1$, $\delta \phi_2$, and δn are arbitrary, thus implying the counterion association/dissociation equilibrium conditions

$$f'_{\text{BW}}(\phi_1) = \lambda - \Lambda - \Psi(0), \quad f'_{\text{BW}}(\phi_2) = \lambda - \Lambda - \Psi(d) \quad (5)$$

at the two macroion surfaces (recall that the prime in $f'_{\text{BW}}(\phi_1)$ and $f'_{\text{BW}}(\phi_2)$ denotes the derivative with respect to the argument) as well as the Boltzmann distribution $n = e^{-\Psi - \Lambda/\nu}$.

Note that the association/dissociation reaction $S^- + A^+ \rightleftharpoons SA$, which we may consider taking place on macroion surface “1” (located at $x = 0$), implies surface fractions of neutral and anionic sites $[SA] = \phi_1$ and $[S^-] = 1 - \phi_1$, respectively, as well as a local counterion concentration at the surface $[A^+] = n(0)$. Inserting $\Lambda = -\Psi(0) - \ln[\nu n(0)]$ from the Boltzmann distribution at $x = 0$ into eqn (5) and assuming $\chi = 0$, yields the equilibrium constant

$$K = \frac{[SA]}{[S^-][A^+]} = \frac{\phi_1}{1 - \phi_1 n(0)} = \nu e^\lambda \quad (6)$$

of the association/dissociation reaction. Eqn (6) is valid in the presence or absence of electrostatic interactions, and their absence entails $n(0) = (1 - \phi)/(ad)$ is uniform. If non-ideal behavior is present ($\chi \neq 0$), the surface fractions $[SA] = \phi_1$ and $[S^-] = 1 - \phi_1$ are to be multiplied by corresponding activity coefficients.

Inserting the Boltzmann distribution $n = e^{-\Psi - \Lambda/\nu}$ into Poisson's equation yields the Poisson–Boltzmann equation $\Psi'' = -(\kappa^2/2) \times e^{-\Psi}$, where we have defined κ through $\kappa^2 = 8\pi l_B e^{-\Lambda/\nu}$. The solution of the Poisson–Boltzmann equation for planar geometry in the absence of salt can be expressed as

$$\Psi(x) = 2 \ln \left\{ \cos \left[\frac{\kappa}{2} \left(x - \frac{d + \delta}{2} \right) \right] \right\}. \quad (7)$$

The length δ will vanish for a symmetric state where $\phi_1 = \phi_2$, but not when the symmetry is broken and $\phi_1 \neq \phi_2$. From eqn (7) we can calculate $\Psi(0)$ and $\Psi(d)$, which appear in eqn (5) as well as $\Psi'(0)$ and $\Psi'(d)$, which enter the electrostatic boundary conditions implied by Poisson's equation, $\Psi'(0)/(4\pi l_B) = (1$



– ϕ_1/a and $\Psi'(d)/(4\pi l_B) = -(1 - \phi_2)/a$. To proceed, we introduce the convenient notation $B = a/(4\pi l_B)$ and switch from λ to the new quantity $d_r = (\nu/a) \times e^\lambda$. Both B and d_r carry a positive sign and have the dimension of a length. Note that $B = (1 - \phi)l_{GC}/2$ is related to the Gouy–Chapman length³⁹ l_{GC} of a macroion surface with a degree of counterion association ϕ . The two electrostatic boundary conditions together with the counterion association/dissociation equilibria in eqn (5) then give rise to four algebraic equations

$$\begin{aligned}\phi_1 &= 1 - B\kappa \tan\left[\frac{\kappa}{4}(d + \delta)\right], \\ \phi_2 &= 1 - B\kappa \tan\left[\frac{\kappa}{4}(d - \delta)\right], \\ \ln\frac{d_r B \kappa^2}{2} &= f'_{BW}(\phi_1) + 2 \ln\left\{\cos\left[\frac{\kappa}{4}(d + \delta)\right]\right\}, \\ \ln\frac{d_r B \kappa^2}{2} &= f'_{BW}(\phi_2) + 2 \ln\left\{\cos\left[\frac{\kappa}{4}(d - \delta)\right]\right\},\end{aligned}\quad (8)$$

which define the four unknown quantities ϕ_1 , ϕ_2 , κ , and δ as function of the parameters B , d , d_r , and χ . Our goal is to obtain a complete understanding of the solutions eqn (8) offer. To this end, it is convenient to measure lengths in units of B . That is, we define the scaled quantities $\bar{d} = d/(4B) = \pi l_B d/a$ and $\bar{d}_r = d_r/(4B) = \pi l_B \nu e^\lambda/a^2$. In addition, we define the auxiliary dimensionless quantities

$$C_1 = \cos\left[\frac{\kappa}{4}(d + \delta)\right], \quad C_2 = \cos\left[\frac{\kappa}{4}(d - \delta)\right], \quad (9)$$

allowing us to express eqn (8) in terms of \bar{d} , \bar{d}_r , C_1 , C_2 through

$$\begin{aligned}f_1(\phi_1, \phi_2) &= 2\bar{d}(1 - \phi_1) - \frac{\sqrt{1 - C_1^2}}{C_1}(\arccos C_1 + \arccos C_2) = 0, \\ f_2(\phi_1, \phi_2) &= 2\bar{d}(1 - \phi_2) - \frac{\sqrt{1 - C_2^2}}{C_2}(\arccos C_1 + \arccos C_2) = 0,\end{aligned}\quad (10)$$

with

$$\begin{aligned}C_1 &= \sqrt{1 - 2\bar{d}_r(1 - \phi_1)^2 \exp[-f'_{BW}(\phi_1)]}, \\ C_2 &= \sqrt{1 - 2\bar{d}_r(1 - \phi_2)^2 \exp[-f'_{BW}(\phi_2)]}.\end{aligned}\quad (11)$$

Inserting C_1 and C_2 into eqn (10) enables us to compute ϕ_1 and ϕ_2 based on solving only two algebraic equations, $f_1(\phi_1, \phi_2) = 0$ and $f_2(\phi_1, \phi_2) = 0$. Each equation defines a relationship, $\phi_1 = \phi_1(\phi_2)$, that can be viewed as a curve in a ϕ_1, ϕ_2 -diagram. Because of the symmetry $f_1(\phi_1, \phi_2) = f_2(\phi_2, \phi_1)$, the two curves are inverse to each other; that is, their graphs are mirror images across the line $\phi_1 = \phi_2$. Once ϕ_1 and ϕ_2 have been

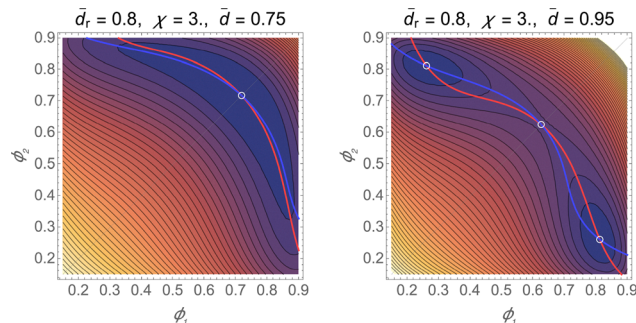


Fig. 2 Degrees of counterion association, ϕ_1 and ϕ_2 , depend on \bar{d}_r , χ , \bar{d} . The two diagrams show results for $\bar{d}_r = 0.8$ and $\chi = 3.0$, with $\bar{d} = 0.75$ (left diagram) and $\bar{d} = 0.95$ (right diagram). Each diagram displays solutions of eqn (10), the red line for the upper and blue line for the lower equation, with intersections locating the stationary points (marked by white circles). Also shown is the corresponding free energy $F \times a/A$ in eqn (2) by a contour plot, with darker colors for lower free energy values. A thin gray line marks the main diagonal where $\phi_1 = \phi_2$. Red and blue lines in each diagram are mirror images of each other with respect to that line. The stationary point on the line $\phi_1 = \phi_2$ corresponds to a minimum in the left diagram and to a saddle point in the right diagram.

calculated, C_1 and C_2 follow from eqn (11), allowing us to determine from eqn (9)

$$\begin{aligned}\kappa &= \frac{2}{d}(\arccos C_1 + \arccos C_2), \\ \delta &= d \frac{\arccos C_1 - \arccos C_2}{\arccos C_1 + \arccos C_2}.\end{aligned}\quad (12)$$

This fully defines the solution $\Psi(x)$ as function of d in eqn (7) and thus allows us to compute all other system properties, including the free energy F . An example is displayed in Fig. 2 for $\bar{d}_r = 0.8$, $\chi = 3.0$ and the two different values $\bar{d} = 0.75$ (left diagram) and $\bar{d} = 0.95$ (right diagram). We show solutions of eqn (10) (the red line for the upper and blue line for the lower equation), with white circles marking their intersections and thus the stationary points of the free energy. Also shown are contour lines that represent the free energy $F \times a/A$, with darker colours indicating lower free energy. Clearly, the symmetric solution $\phi_1 = \phi_2$ represents a minimum of the free energy for $\bar{d} = 0.75$ whereas it has turned into a saddle point for $\bar{d} = 0.95$. The minima of the free energy are now located at asymmetric states $\phi_1 \neq \phi_2$, indicating a symmetry breaking transition has taken place. Let us analyze that transition systematically.

3 Perturbation approach

For $\phi_1 = \phi_2$ both macroions carry the same effective charge. The solution $\Psi(x)$ in eqn (7) is then mirror-symmetric with respect to the plane $x = d/2$, implying $\delta = 0$. Eqn (10) always possess a symmetric solution $\phi_s = \phi_1 = \phi_2$ but the corresponding stationary point may locate a minimum or a saddle point of the free energy. The transition from the former to the latter marks an instability that we can identify by a perturbation approach. We insert $\phi_1 = \phi_s + \Delta\phi$ and $\phi_2 = \phi_s - \Delta\phi$ into eqn (10)–(11).



Sufficiently small $\Delta\phi$ then gives rise to the two relations

$$\bar{d}_r = \frac{2\chi\phi_s(1-\phi_s) - 1}{4(1-\phi_s)^3} e^{\chi(1-2\phi_s)}, \quad (13)$$

$$\bar{d} = \frac{\sqrt{\chi(1-\phi_s) - \frac{1}{2\phi_s}} \arccos\left(\frac{\sqrt{1-\chi(1-\phi_s) + \frac{1}{2\phi_s}}}{\sqrt{1-\chi(1-\phi_s) + \frac{1}{2\phi_s}}}\right)}{1-\phi_s}$$

which fully characterize the transition between symmetric states (where $\phi_1 = \phi_2$) corresponding to a local minimum and a saddle point. Eqn (13) represents a central result of this study, as the two relationships fully characterize the local stability of the symmetric state.

The upper diagram in Fig. 3 shows \bar{d}_r and \bar{d} as function of ϕ_s for fixed $\chi = 3.0$. For any given value $\bar{d}_r < 1$ (which is marked by the blue circle), two distinct degrees of counterion association ϕ_s^A and ϕ_s^B with corresponding scaled distances $\bar{d}^A = \bar{d}(\phi_s^A)$ and $\bar{d}^B = \bar{d}(\phi_s^B)$ between the two macroions are predicted. Shown in the diagram is the specific choice $\bar{d}_r = 0.8$, entailing $\phi_s^A = 0.3442$ and $\phi_s^B = 0.6771$ as well as $\bar{d}^A = 1.2569$ and $\bar{d}^B = 0.8475$. Recall that the two contour plots in Fig. 2 were calculated for $\chi = 3.0$ and $\bar{d}_r = 0.8$, with a minimum of the symmetric state for $\bar{d} = 0.75$ and a saddle point for $\bar{d} = 0.95$. Fig. 3 predicts the transition

from local minimum to saddle point to take place at $\bar{d} = \bar{d}^B = 0.8475$. Moreover, another transition back to a local minimum occurs at $\bar{d} = \bar{d}^A = 1.2569$.

The critical point, $\phi_s = 1/2$ and $\bar{d}_r = 1$, in the upper diagram of Fig. 3 is marked by a blue circle, which applies to $\chi = 3$. No asymmetric equilibrium states exist for values $\bar{d}_r > 1$. Because of $\bar{d}_r \sim e^\chi$, it follows that sufficiently large counterion association energies λ prevent the formation of asymmetric equilibrium states $\phi_1 \neq \phi_2$. Different values of χ lead to different critical points, which is shown in the lower diagram of Fig. 3. The gray line connecting the critical points for different χ follows the relationship

$$\chi = \frac{2 + \phi_s \pm \sqrt{[\phi_s - 2(2 + \sqrt{3})][\phi_s - 2(2 - \sqrt{3})]}}{4\phi_s(1 - \phi_s)}, \quad (14)$$

with the plus and minus signs applying to values of χ larger and smaller than $\chi = (5 + 3\sqrt{3})/4 \approx 2.5490$, respectively. The corresponding $\phi_s = 2(2 - \sqrt{3}) \approx 0.5359$ marks the largest possible value for the onset of the asymmetry transition, and this is accompanied by $\bar{d}_r = 0.5580$ and $\bar{d} = (2 + \sqrt{3})\pi/18 \approx 0.6514$. No critical point can have a degree of counterion association larger than $\phi_s = 2(2 - \sqrt{3}) \approx 0.5359$.

We also note the two critical values $\chi = 3$ and $\chi = 2$ for $\phi_s = 1/2$. The former, $\chi = 3$, implies $\bar{d}_r = 1$ and $\bar{d} = \pi/2$. The latter, $\chi = 2$, is the lowest value above which asymmetric states can exist. This occurs in the limit where both $\bar{d}_r \rightarrow 0$ and $\bar{d} \rightarrow 0$. Here, electrostatic interactions are irrelevant, and since half the counterions are adsorbed, the critical point $\phi_s = 1/2$ and $\chi = 2$ is predicted entirely by the Bragg-Williams free energy in eqn (1).

4 Characterization of symmetry breaking

The perturbation approach above informs us that asymmetric states must exist if the symmetric state corresponds to a saddle point of the free energy. Yet, asymmetric states may even exist if the symmetric state falls into a local minimum of the free energy. In this case, a contour plot such as in Fig. 2 would have five stationary points, three local minima of the free energy separated by two saddle points. This can indeed be observed and has thus been studied by identifying all local free energy minima for choices of the three parameters, \bar{d}_r , \bar{d} , and χ . In Fig. 4 we show diagrams of ϕ_1 and ϕ_2 as function of \bar{d} for fixed $\bar{d}_r = 0.8$ and four different values of χ .

Fig. 4A, which is calculated for $\chi = 3.0$, demonstrates the existence of a region with a metastable symmetric minimum and a stable asymmetric minimum between the values $\bar{d}_s^A = 0.7992$ and $\bar{d}^A = 0.8475$ and then again between $\bar{d}^B = 1.2569$ and $\bar{d}_s^B = 1.2806$ as the scaled macroion-to-macroion distance \bar{d} is increased. Two local minima of the free energy are always separated by a saddle point. The locations of all saddle points in Fig. 4 are shown as dashed lines. The four blue circles in Fig. 4A mark the stationary points for $\bar{d} = 0.75$ (one point) and $\bar{d} = 0.95$ (three points), which are consistent with the two

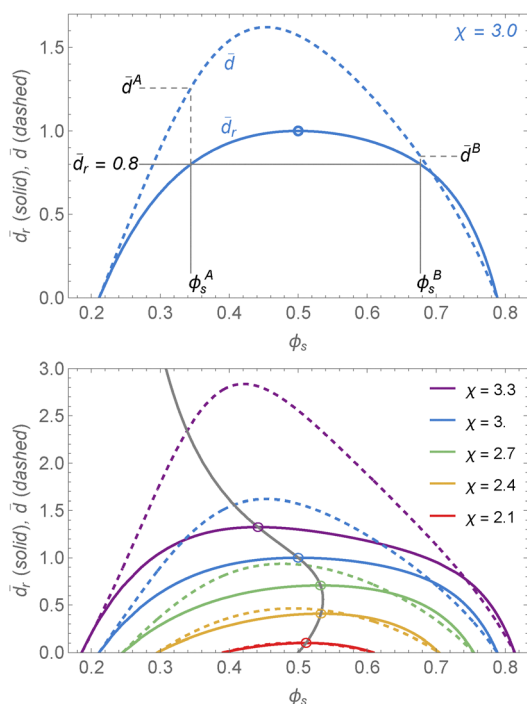


Fig. 3 The functions $\bar{d}_r(\phi_s)$ (solid lines) and $\bar{d}(\phi_s)$ (dashed lines) according to eqn (13). The upper diagram focuses on $\chi = 3.0$, showing specific values of ϕ_s^A and ϕ_s^B at positions where $\bar{d}_r = 0.8$. Corresponding scaled distances $\bar{d}^A = \bar{d}(\phi_s^A)$ and $\bar{d}^B = \bar{d}(\phi_s^B)$ are marked. The small circle locates the critical point $\phi_s = 1/2$ and $\bar{d}_r = 1$. The lower diagram includes five different values of χ as indicated in the legend. Critical points are marked by color-matching small circles. The gray solid line shows the progression of the critical points according to eqn (14).



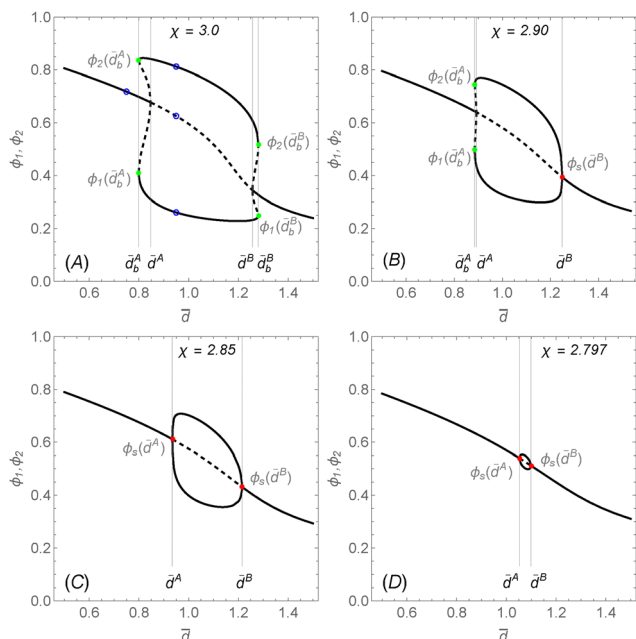


Fig. 4 Degrees of counterion association, ϕ_1 and ϕ_2 , as function of the scaled macroion-to-macroion distance \bar{d} for fixed $\bar{d}_r = 0.8$ and four different values of χ as stated on top of diagrams A–D. States residing in local minima and at saddle points of the free energy are displayed by solid lines and dashed lines, respectively. Onsets of discontinuous and continuous transitions are marked by green and red bullets, respectively. Corresponding thin vertical lines assist in locating the positions \bar{d}_b^A , \bar{d}^A , \bar{d}^B , and \bar{d}_b^B . The four blue circles in diagram A mark the stationary points at $\bar{d} = 0.75$ and $\bar{d} = 0.95$ that correspond to the free energy contours in Fig. 2.

diagrams in Fig. 2. We emphasize that the transitions from stable symmetric to stable asymmetric states in Fig. 4A at $\bar{d} = \bar{d}_b^A$ and $\bar{d} = \bar{d}_b^B$ are both discontinuous. They can be located by finding solutions of $f_1(\phi_1, \phi_2) = 0$ and $f_2(\phi_1, \phi_2) = 0$ such that the additional condition

$$\frac{\partial f_1}{\partial \phi_2} \frac{\partial f_2}{\partial \phi_1} = \frac{\partial f_2}{\partial \phi_2} \frac{\partial f_1}{\partial \phi_1} \quad (15)$$

ensures that two inverse curves intersect each other tangentially. The three equations specify \bar{d} , ϕ_1 , ϕ_2 for any given \bar{d}_r and χ . For $\chi = 3.0$, two such solutions exist, denoted by \bar{d}_b^A , $\phi_1(\bar{d}_b^A)$, $\phi_2(\bar{d}_b^A)$, and \bar{d}_b^B , $\phi_1(\bar{d}_b^B)$, $\phi_2(\bar{d}_b^B)$ and marked in Fig. 4A by green bullets.

The discontinuous nature of the symmetry breaking transition persists upon lowering χ until at $\chi = 2.9149$ the locations \bar{d}_b^B and \bar{d}^B merge. Below $\chi = 2.9149$, the point \bar{d}_b^B does not exist, leaving only \bar{d}^B to mark the onset of the transition, which is now continuous. For $\chi = 2.90$, this is displayed in Fig. 4B. The red bullet at \bar{d}^B marks the continuous transition. Note that the two values $\bar{d}_b^A = 0.8851$ and $\bar{d}^A = 0.8923$ remain distinct, implying one of the two transitions is still discontinuous. Below $\chi = 2.8562$ both transitions become continuous and are predicted by eqn (13) (see also Fig. 3). The values of $\chi(\bar{d}_r)$, where the transition from a discontinuous jump to a smooth symmetry breaking takes place, cannot be determined from eqn (13). We have computed them numerically. Fig. 4C was calculated for

$\chi = 2.85$, where both symmetry-breaking transitions occur in a continuous manner.

Decreasing χ even further renders the range of transition, from \bar{d}^A to \bar{d}^B , smaller until at $\chi = 2.7958$ it ceases to exist. The critical point $\chi = 2.7958$ is predicted by eqn (13). In the lower diagram of Fig. 3 it would be the critical point for the curve at $\chi = 2.7958$, leading to $\bar{d}_r = 0.8$ with $\phi_s = 0.5260$ and $\bar{d} = 1.0756$. That curve falls between the displayed curves for $\chi = 2.7$ and $\chi = 3.0$. Fig. 4D shows the case $\chi = 2.797$, barely above the critical point and thus leading to a narrowly confined region in which symmetry breaking takes place. No metastable regions are present in Fig. 4C and D.

5 Stability diagram

Recall that our model is completely defined by the three dimensionless parameters $\bar{d}_r = \pi l_B \nu e^2 / a^2$, $\bar{d} = \pi l_B d / a$, and χ , expressing the counterion association strength λ , the macroion-to-macroion distance d , and the non-ideality parameter χ . Hence, our model's predictions can be cast into a three-dimensional stability diagram, which includes regions of local instability and metastability. This diagram is displayed in Fig. 5. Regions enclosed by solid lines have locally unstable symmetric states, implying symmetry breaking must occur. They are fully defined by eqn (13). Regions between color-matching solid and dashed lines are metastable: their symmetric states reside in a local but not in a global free energy minimum. The largest value of $\bar{d}_r = \bar{d}_r(\chi)$ that leads to an instability gives rise to a critical point, marked by circles in Fig. 5. Close to the critical point, no metastable regions exist.

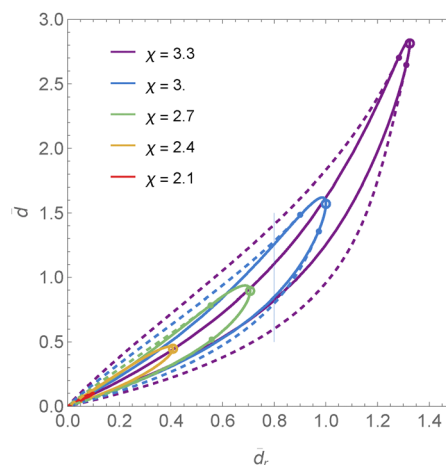


Fig. 5 Stability diagram, indicating regions of spontaneous symmetry breaking as function of \bar{d}_r and \bar{d} for different values of χ as specified in the legend. Regions enclosed by solid lines have locally unstable symmetric states. Regions between solid and dashed lines have metastable symmetric states. Open circles mark critical points, beyond which asymmetric states (with larger \bar{d}_r) do not exist. No metastable states are present near critical points. Small bullets (for clarity shown only for $\chi = 2.7, 3.0$, and 3.3) mark the beginning of the metastable regions. The thin blue vertical line shows the path along which the degrees of counterion association, ϕ_1 and ϕ_2 , are shown in Fig. 4A.



They appear only below values for \bar{d}_r and \bar{d} marked by small bullets in Fig. 5. The locations of these small bullets explain when diagrams such as Fig. 4B exist, where one transition is continuous and the other discontinuous. The thin vertical blue line in Fig. 5 indicates the pathway, from $\bar{d} = 0.5$ to $\bar{d} = 1.5$ at fixed $\bar{d}_r = 0.8$ and $\chi = 3.0$, along which Fig. 4A was calculated. Here, stable and unstable symmetric states along this path are separated by two metastable regions, bounded by \bar{d}_b^A , \bar{d}^A and \bar{d}^B , \bar{d}_b^B . Using the stability diagram in Fig. 5, it is straightforward to predict if a given path intersects with zero, one, or two metastable regions.

Fig. 5 indicates that the region in which symmetry breaking occurs is always confined to a finite range, $0 < d < \infty$, and does not extend to either contact ($d = 0$) or infinite separation ($d \rightarrow \infty$). In the limit $d \rightarrow 0$, the degree of counterion association approaches $\phi \rightarrow 1$ for any finite association energy $-\infty < \lambda < \infty$, driving the system close to full association (or, equivalently, zero dissociation). This proximity to $\phi = 1$ suppresses the formation of asymmetric states due to the high entropy penalty. In the opposite limit $d \rightarrow \infty$, symmetry breaking is absent because isolated, non-interacting macroions are assumed to be stable, an assumption that will be examined further in Section 6.4.

6 Discussion

Our theoretical model provides a description of spontaneous symmetry breaking of two interacting, chemically identical, planar macroions that are subject to charge regulation based on a non-ideal counterion association/dissociation isotherm according to the mean-field Bragg-Williams free energy in eqn (1). Each charge on the macroion is the result of a dissociation reaction that produces a mobile counterion. No salt is present, implying that only counterions reside between the two macroion surfaces. In the following, we discuss the applicability of our no-salt assumption, specify experimental conditions to which our model applies, investigate the role of electrostatic interactions for the spontaneous symmetry breaking, identify a maximal value of χ below which an isolated macroion remains stable, calculate the disjoining pressure between the interacting macroions, and compare our model with preceding work by Majee *et al.*³⁴

6.1 Applicability of the no-salt assumption

A crucial assumption of our model is the absence of salt. Salt, which is always present to some extent, gives rise to a characteristic length, the Debye length l_D , beyond which interactions are screened. The presence of salt can be neglected if interactions between macroions occur on length scales much smaller than l_D . To illustrate this point, we consider a single charged planar surface carrying a fixed negative surface charge density $\sigma = -e/a$ in contact with a symmetric 1:1 electrolyte. The Debye length $l_D = 1/\sqrt{8\pi l_B n_0}$ reflects the presence of salt with bulk concentration n_0 . We solve the corresponding Poisson-Boltzmann equation $l_D^2 \Psi''(x) = \sinh \Psi(x)$ subject to the

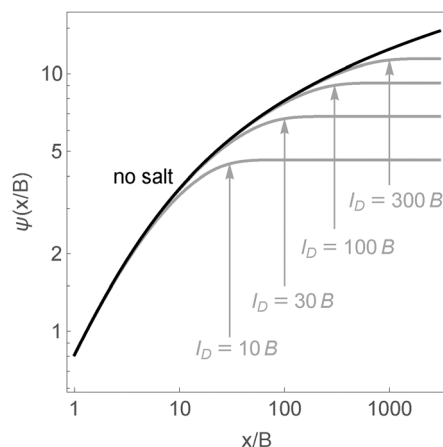


Fig. 6 Log-log plot of the potential $\Psi(x/B)$ as function of the scaled distance x/B (with $B = a/(4\pi l_B)$) away from a single planar macroion surface in contact with a symmetric 1:1 electrolyte of scaled Debye length l_D/B . The four gray curves labeled by the arrows in the diagram correspond to $l_D = 10B$, $l_D = 30B$, $l_D = 100B$, and $l_D = 300B$. For distances $x \ll l_D$, the potential for the Poisson-Boltzmann model in the absence of salt, $\Psi(x) = 2 \ln[1 + x/(2B)]$ (shown as a black solid line) reproduces the potential for the Poisson-Boltzmann model in the presence of salt.

boundary conditions $\Psi(0) = 0$ and $\Psi'(0) = 4\pi l_B/a = 1/B$ at the macroion surface $x = 0$. Inside the bulk of the electrolyte, for $x \rightarrow \infty$, the potential will be constant and equal to the potential difference produced by the electric double layer. It is convenient to use the length B as unit length. The gray curves in Fig. 6 show Ψ as function of x/B for different values of the scaled Debye length l_D/B . As l_D/B grows, the potential $\Psi(x) = 2 \ln[1 + x/(2B)]$ is increasingly better approximated inside the region $0 \leq x \ll l_D$. Yet, $\Psi(x) = 2 \ln[1 + x/(2B)]$ is exactly the potential produced by the Poisson-Boltzmann model in the absence of salt, solving $\Psi''(x) = -(\kappa^2/2) \times e^{-\Psi(x)}$ with $\Psi(0) = 0$ and $\Psi'(0) = 1/B$. Hence, at distances much smaller than l_D away from a single charged surface, the use of the Poisson-Boltzmann model in the absence of added salt is justified.

These considerations can be extended to the interaction between two planar surfaces with charge densities $\sigma = -e/a$. For separations $d \ll l_D$, the potential $\Psi(x) = \Psi(d/2) - (x - d/2)^2/(Bd)$ with $\Psi(d/2) = -\ln[4l_D^2/(Bd)]$ satisfies the Poisson-Boltzmann equation $l_D^2 \Psi''(x) = \sinh \Psi(x)$ together with the boundary conditions $\Psi'(0) = -\Psi'(d) = 1/B$ at the two macroion surfaces located at $x = 0$ and $x = d$. Apart from the irrelevant constant $\Psi(d/2)$, the same potential is obtained from eqn (7) for the salt-free model in the limit $d \ll l_D$. This limit corresponds to the so-called ideal-gas regime,⁴⁰ which yields $\kappa^2 = 4/(Bd)$.

6.2 Discussion of experimental relevance

The stability diagram in Fig. 5 indicates that if spontaneous symmetry breaking occurs, the dimensionless separation $\bar{d} \approx 1$ will be of order unity. As discussed below in Section 6.4, for $\chi > 2 + \sqrt{3} \approx 3.732$ an isolated macroion becomes unstable with respect to internal phase separation, resulting in spatially heterogeneous counterion association along the macroion surface. Only for values of χ slightly below this threshold can



spontaneous symmetry breaking occur at large, but not infinitely large, separations $1 \ll \bar{d} < \infty$. For example, at $\chi = 3.7$, the largest separation at which symmetry breaking can occur is $\bar{d} = 8$. The characteristic value $\bar{d} = \pi l_B d/a \approx 1$ implies, roughly, a physical separation $d \sim a/l_B$ for the onset of symmetry breaking. Consequently, we expect our present salt-free theoretical predictions to become experimentally testable for salt concentrations with corresponding Debye length $l_D \gg a/l_B$. Typical charge densities of macroions have magnitudes $|e/a|$ with a varying by two orders of magnitude, from $a \approx 100 \text{ nm}^2$ for silica particles near neutral pH, weakly functionalized latex particles, weakly charged lipid membranes, and microgels under weak ionization, to $a \approx 1 \text{ nm}^2$ for DNA, cytoskeletal filaments, viral capsids, and highly charged lipid membranes.³⁹ Assuming a Bjerrum length of order $l_B = 1 \text{ nm}$ we arrive at salt concentrations significantly smaller than $10 \text{ }\mu\text{M}$ for weakly charged macroions and significantly smaller than 100 mM for highly charged macroions. We conclude that for a wide range of macroions experimentally accessible salt concentrations exist that can test our present model. For example, recent experiments by Wang *et al.*⁴ employed charged silica particles and aminated silica particles at salt concentrations starting from $5 \text{ }\mu\text{M}$. Under these conditions our model would be applicable if $a \lesssim 100 \text{ nm}^2$. Experimentally supported charge densities of silica particles, including functionalized silica particles, fall well into this range.^{41–43}

Let us connect the dimensionless parameters \bar{d}_r and \bar{d} to values for λ and d using a characteristic experimental scenario. Recall first our definitions $d_r = \nu/a \times e^{\lambda}$, $\bar{d}_r = d_r/(4B)$, $\bar{d} = d/(4B)$, and $B = a/(4\pi l_B)$, which yield $\bar{d}_r = \pi l_B \nu e^{\lambda}/a^2$ and $d = \bar{d}a/(\pi l_B)$. Let us choose $a = 10 \text{ nm}^2$ for the area per dissociable group on the macroion surface, $l_B = 1 \text{ nm}$ for the Bjerrum length, $\chi = 3$ for the non-ideality parameter, and $\lambda = 0.24$ for the adsorption strength. The volume ν sets a reference for measuring λ . Specifically $\lambda = 0$ and $\chi = 0$ yield a 50%-degree of association/dissociation at a distance $d = \nu/(2a)$ in the absence of electrostatic interactions. Choosing $\nu = 20 \text{ nm}^3$ sets that distance to be $d = 1 \text{ nm}$. With that we obtain $\bar{d}_r = 0.8$. From Fig. 4A we recall the region $0.8 < \bar{d} < 1.28$ for spontaneous symmetry breaking. This then translates into a range $2.5 \text{ nm} < d < 4.1 \text{ nm}$ of macroion-to-macroion distances at which our model predicts symmetry breaking. Applicability of this example would require a Debye screening length of $l_D \gg a/l_B = 10 \text{ nm}$ and thus a salt concentration of much less than 1 mM .

We finally note that while our model refers to the planar macroion geometry, it can also be applied to spherical colloids using the Derjaguin approximation,^{39,44} given the radius of the colloid $R \gg l_D$ is much larger than the Debye screening length l_D .

6.3 Role of electrostatic interactions

In the following, we aim to understand the role electrostatic interactions play for the spontaneous symmetry breaking. Would “switching off” the Coulomb interaction between all involved charges suppress or enhance the occurrence of

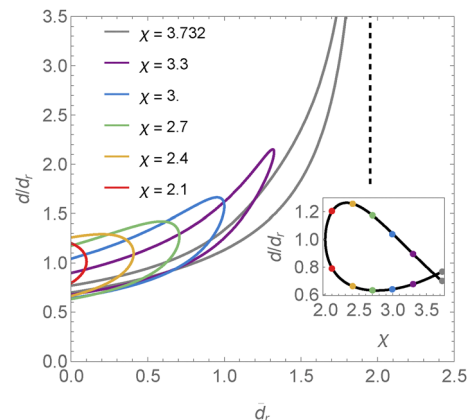


Fig. 7 Regions inside which symmetric states are locally unstable, re-plotted from Fig. 4 as function of d/d_r and $\bar{d}_r = \pi l_B d_r/a$ for different values of χ as specified in the legend. The absence of electrostatic interactions ($l_B \rightarrow 0$) corresponds to the line $\bar{d}_r = 0$. For $\chi > 2 + \sqrt{3} \approx 3.732$ an isolated planar macroion becomes unstable, with the instability occurring first at $\bar{d}_r = (3 + 2\sqrt{3}) \times e/9 \approx 1.952$, indicated by the dashed vertical black line. The inset shows d/d_r as function of χ in the absence of electrostatic interactions. The colored bullets match the curves shown in the main diagram at position $\bar{d}_r = 0$.

symmetry breaking? This can be investigated by ignoring the electrostatic energy term $\Psi^{1/2}/(8\pi l_B)$ in eqn (2). The counterions, which now do no longer carry an electric charge, distribute uniformly between the two uncharged plates. Changing the plate-to-plate distance d still affects the degree of adsorption ϕ_1 and ϕ_2 . In fact, the two equations $d/d_r = (2 - \phi_1 - \phi_2)e^{-f_{BW}(\phi_1)}$ and $d/d_r = (2 - \phi_1 - \phi_2)e^{-f_{BW}(\phi_2)}$ specify ϕ_1 and ϕ_2 for any stationary state of the free energy. The absence of electrostatics implies $l_B \rightarrow 0$. The length $B = a/(4\pi l_B)$ therefore diverges and thus can no longer be used to scale other quantities. Instead, the ratio d/d_r emerges as a convenient dimensionless quantity to characterize the onset of spontaneous symmetry breaking. A perturbation calculation analogous to that in Section 4 shows that in between the two values $d/d_r = 2(\chi - 1 + s)/(\chi - s)e^{-s}$ with $s = \pm\sqrt{\chi(\chi - 2)}$, the symmetric state is unstable. The two values of d/d_r are plotted in the inset of Fig. 7. To directly compare the instability regions in the absence and presence of electrostatic interactions, we re-plot the regions inside which symmetric states are locally unstable from Fig. 5 as function of d/d_r instead of \bar{d} . This is shown in the main diagram of Fig. 7. Recall the horizontal axis shows $\bar{d}_r = d_r/(4B)$ with $B = a/(4\pi l_B)$, implying $\bar{d}_r = \pi l_B d_r/a$. The strength of the Coulomb potential is proportional to the Bjerrum length l_B , implying $\bar{d}_r \rightarrow 0$ in the absence of electrostatic interactions. This corresponds to the instability region on the left axis of Fig. 7. For example, the red curve, for $\chi = 2.1$, implies $d/d_r = 1.200$ and $d/d_r = 0.7933$ in the limit $\bar{d}_r = 0$, where electrostatic interactions are absent. These two points appear in the inset of Fig. 7 at the same positions and are marked by the two red bullets. Instability points for other values of χ are marked by color-matching bullets. Fig. 7 reveals the behavior implied by “switching on” electrostatic interactions corresponds to moving horizontally through the



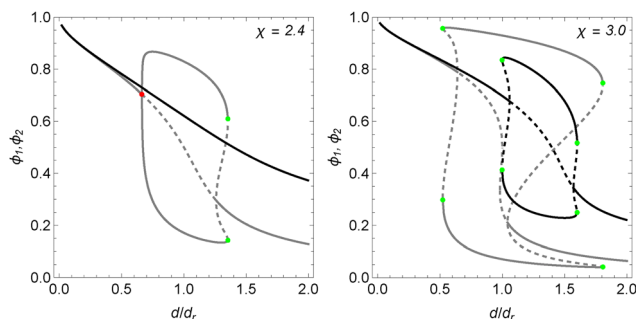


Fig. 8 Degrees of counterion association, ϕ_1 and ϕ_2 , as function of the scaled macroion-to-macroion distance d/d_r for fixed $\bar{d}_r = 0.8$ as well as $\chi = 2.4$ (left diagram) and $\chi = 3.0$ (right diagram). Black and gray lines refer to the presence and absence of electrostatics, respectively. Solid lines correspond to states that are locally stable, dashed lines characterize stationary points of the free energy that are unstable. Green and red bullets mark discontinuous and continuous transitions between symmetric ($\phi_1 = \phi_2$) and asymmetric ($\phi_1 \neq \phi_2$) degrees of counterion association. The black lines in the right diagram, which are computed for $\bar{d}_r = 0.8$ and $\chi = 3.0$ in the presence of electrostatic interactions, represent the same data as in Fig. 4A.

stability diagram, starting at $\bar{d}_r = 0$. This assumes all other parameters (χ and λ) remain fixed. If a system is unstable at $\bar{d}_r = 0$, it will always move into a stable region. If it is not stable at $\bar{d}_r = 0$, it may pass through a region of instability, but eventually end up in a stable region. In this sense, electrostatic interactions do not tend to induce spontaneous symmetry breaking. Instead, they stabilize the symmetric state, $\phi_1 = \phi_2$.

We exemplify the predictions of Fig. 7 by a comparison of the degrees of counterion association, ϕ_1 and ϕ_2 , in the absence and presence of electrostatic interactions for two specific cases shown in Fig. 8, with $\chi = 2.4$ (left diagram) and $\chi = 3.0$ (right diagram). The black lines show ϕ_1 and ϕ_2 in the presence of electrostatics with $\bar{d}_r = 0.8$ as in Fig. 4. The gray lines refer to the absence of electrostatic interactions, where $B \rightarrow \infty$. Note that Fig. 7 and 8 make consistent predictions: for $\chi = 2.4$, the presence of electrostatic interactions inhibits symmetry breaking, whereas for $\chi = 3.0$ the region of symmetry breaking is shifted to somewhat larger d/d_r .

6.4 Stability of an isolated macroion

Throughout this work we have considered values of χ in the range from $2 < \chi \leq 3.3$. If χ is significantly larger, even an isolated macroion will undergo an instability and phase separate into regions with different degrees of counterion association. Let us find the largest χ for which a single macroion is still stable. Repeating the theoretical approach of the present work for an isolated macroion with a degree of counterion association ϕ leads to the equation

$$\ln\left(\frac{\phi}{2\bar{d}_r(1-\phi)^3}\right) + \chi(1-2\phi) = 0, \quad (16)$$

where we recall $\bar{d}_r = \pi l_B \nu e^2/a^2$. Eqn (16) predicts a critical point $\chi = 2 + \sqrt{3} \approx 3.732$, $\bar{d}_r = (3 + 2\sqrt{3}) \times e/9 \approx 1.952$, and $\phi = (\sqrt{3} - 1)/2 \approx 0.3660$. At the critical point, two solutions

for ϕ will emerge from eqn (16) upon any small increase of χ . We conclude that only for $\chi < 3.732$ does an isolated macroion remain stable against an internal phase transition that would result in spatially inhomogeneous values of ϕ . To place this prediction into the context of the present work, we have added a curve (the gray line) for $\chi = 3.732$ to the stability diagram in Fig. 7. This is the smallest χ for which the instability region grows to infinitely large values of d/d_r , and the divergence occurs at $\bar{d}_r = 1.952$ (marked by the dashed vertical black line in Fig. 7), exactly as predicted by eqn (16). At this point, an isolated macroion surface becomes unstable with respect to the separation into domains with different degrees of counterion association.

Yet another line of context can be established by considering a single planar macroion surface of fixed degree of counterion association ϕ in the presence of salt with corresponding Debye length l_D , as in Fig. 6. Such a surface with fixed charge density $\sigma = -(1 - \phi)e/a$ gives rise to a spinodal line^{45,46}

$$\chi = \frac{1}{2\phi(1-\phi)} + \frac{1}{\sqrt{(2B/l_D)^2 + (1-\phi)^2}} \quad (17)$$

The critical point predicted by eqn (17) increases from $\chi = 2$ and $\phi = 1/2$ in the limit of large salt content ($l_D \rightarrow 0$) to $\chi = 2 + \sqrt{3} \approx 3.732$ and $\phi = (\sqrt{3} - 1)/2 \approx 0.3660$ in the limit of no salt content ($l_D \rightarrow \infty$), exactly as the critical point that emerges from eqn (16) in the presence of charge regulation. The critical point $\chi = 3.732$ for a non-interacting planar surface in the absence of salt was first noted by Gelbart and Bruinsma.⁴⁷ In summary, the range of χ values considered in this work is well justified, since only for $\chi < 3.732$ is an isolated, non-interacting planar macroion surface guaranteed to remain stable with respect to phase separation.

We point out that interacting macroions may adopt non-homogeneous degrees of counterion association even for $2 < \chi < 3.732$. The characterization of these non-homogeneous degrees is outside the scope of the present work. In fact, because the electrostatic contribution to the line tension of two coexisting domains of different surface charge density on a macroion is negative,⁴⁸ the consequence may be the formation of interlocked modulated phases with periodically changing degrees of dissociation along each macroion. Testing this hypothesis may be the subject of a future study.

6.5 Disjoining pressure

The disjoining pressure $P = n(x) - \Psi'(x)^2/(8\pi l_B)$ that acts between the two planar surfaces consists of two contributions, the osmotic pressure of the mobile counterions and the Maxwell stress. Indeed, Beltrami's identity⁴⁹ ensures P emerges as an invariant, independent of x , upon integrating the Poisson-Boltzmann equation $\Psi''' = -(\kappa^2/2) \times e^{-\Psi}$ once. Using $n(x) = e^{-\Psi(x)} \times \kappa^2/(8\pi l_B)$ together with $\Psi(x)$ in eqn (7) leads to $P = \kappa^2/(8\pi l_B)$. For the scaled (dimensionless) pressure $\bar{P} = PaB$ we thus obtain

$$\bar{P} = \frac{(\kappa B)^2}{2} = \frac{1}{2} \left(\frac{\arccos C_1 + \arccos C_2}{2\bar{d}} \right)^2, \quad (18)$$



where C_1 and C_2 follow from eqn (11) after identifying ϕ_1 and ϕ_2 from solving $f_1(\phi_1, \phi_2) = 0$ and $f_2(\phi_1, \phi_2) = 0$ according to eqn (10). Note that the pressure is always positive, indicating the two macroion surfaces always repel each other.

Let us consider the example $\bar{d}_r = 0.8$ and $\chi = 2.85$, discussed in Fig. 4C. Recall there are continuous transitions from the symmetric to the asymmetric state at $\bar{d} = \bar{d}^A$ and then back from the asymmetric to the symmetric state at $\bar{d} = \bar{d}^B$ as \bar{d} increases. For $\bar{d} = \bar{d}^A$ and $\bar{d} = \bar{d}^B$ we obtain $\bar{P} = 0.1850$ and $\bar{P} = 0.1889$, respectively. That is, the pressure increases when increasing the distance between the macroions across the region where $\phi_1 \neq \phi_2$. The full behavior of the scaled pressure as function of the scaled distance $\bar{P} = \bar{P}(\bar{d})$ is shown by the black line (corresponding to $\chi = 2.85$) in Fig. 9 together with red and blue lines for $\chi = 2.9$ and $\chi = 3.0$. Solid and dashed lines correspond to locally stable and unstable states, respectively. The inset shows a magnified view of the region where spontaneous symmetry breaking takes place. Recall from Fig. 4A and B that for $\chi = 2.9$ only one of the two transitions is continuous, the other discontinuous, and for $\chi = 3.0$ both transitions are discontinuous. When the transition is discontinuous, the pressure jumps. Corresponding \bar{d} -values are marked in the inset of Fig. 9 by open circles. In the \bar{d} -region where the macroions have asymmetric degrees of dissociation, the pressure is a non-monotonic function of the distance d . This non-monotonic and in some cases even discontinuous behavior of the pressure is a consequence of the two macroions each being assumed to maintain a spatially uniform degree of counterion association when they interact.

To understand the origin for the non-monotonic pressure, it is important to distinguish between spontaneous symmetry breaking and phase separation. In the former case, each of the two macroions may adopt a different and yet uniform

degree of counterion association over the entire surface. In the latter case, regions with distinct degrees of counterion association grow or shrink, similar to coexisting phases in a phase separation. In the absence of electrostatics, it is straightforward to compare both cases. Recall our discussion of “switching off” electrostatic interactions in Section 6.3, where we have presented in Fig. 8 the degrees of counterion association ϕ_1 and ϕ_2 for the two values $\chi = 2.4$ and $\chi = 3.0$. The gray curves in Fig. 8 refer to the absence of electrostatic interactions. Fig. 10 shows the corresponding (conveniently scaled) disjoining pressure $\bar{P} = Pa d_r = (2 - \phi_1 - \phi_2)d_r/d$ in the absence of electrostatic interactions for the same parameters as in Fig. 8. Here again, dashed lines mark locally unstable states, corresponding to saddle points of the free energy. Gray solid lines refer to stable asymmetric states. The qualitative behavior of \bar{P} is similar in the absence (Fig. 10) and presence (Fig. 8) of electrostatic interactions, changing non-monotonically in the d -region where spontaneous symmetry breaking occurs. For discontinuous symmetry breaking (at positions marked by open circles in Fig. 10), the pressure jumps discontinuously. If we replace the occurrence of symmetry breaking by the ability to phase separate, two phases with different degrees of “counterion” (the counterions are now uncharged) association will coexist on the two surfaces, and the pressure will stay constant when d is changed. The corresponding pressure is determined by the well-known Maxwell construction and indicated in both diagrams of Fig. 10 by a brown horizontal line with two brown triangles locating the d -region where phase separation takes place. Thus, the pressure does not exhibit non-monotonic behavior during a phase transition if electrostatic interactions are absent.

Our consideration of electrostatic interactions being absent makes the distinction between spontaneous symmetry

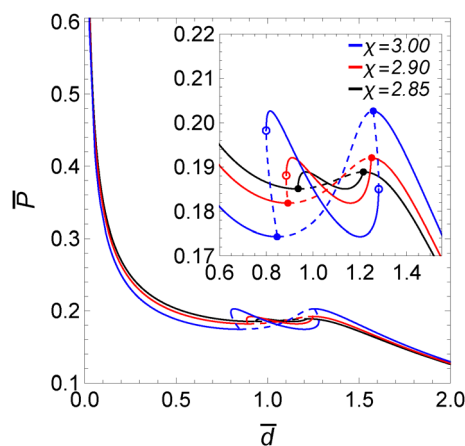


Fig. 9 Scaled disjoining pressure $\bar{P} = PaB$ as function of the scaled distance $\bar{d} = d/(4B) = d \times \pi l_B/a$ for $\bar{d}_r = 0.8$ and $\chi = 3.0$ (blue), $\chi = 2.9$ (red), and $\chi = 2.85$ (black). The three curves correspond to the degrees of counterion association shown in Fig. 4A–C. Solid and dashed lines correspond to locally stable and unstable states, respectively. The inset shows a magnified view of the region where spontaneous symmetry breaking takes place. Dashed lines between bullets mark unstable symmetric states. Open circles locate transitions to the asymmetric state that are discontinuous.

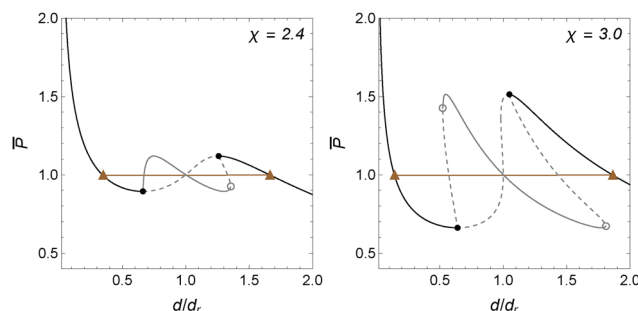


Fig. 10 Scaled disjoining pressure $\bar{P} = Pa d_r = (2 - \phi_1 - \phi_2)d_r/d$ as function of the scaled distance d/d_r for $\chi = 2.4$ (left diagram), and $\chi = 3.0$ (right diagram). No electrostatic interactions are present ($l_B \rightarrow 0$). Recall that $d/d_r = (2 - \phi_1 - \phi_2)e^{-f_{BW}(\phi_1)}$ and $d/d_r = (2 - \phi_1 - \phi_2)e^{-f_{BW}(\phi_2)}$ specify ϕ_1 and ϕ_2 for any stationary state of the free energy. Dashed lines correspond to locally unstable states. Black solid lines mark locally stable symmetric states, gray solid lines stable asymmetric states. Black bullets separate locally unstable and stable symmetric states. Gray open circles mark discontinuous transitions of the pressure, occurring in conjunction with discontinuous symmetry breaking; see Fig. 8. Brown horizontal lines terminating in two brown triangles locate a constant pressure according to the Maxwell construction, as is the case when two phases with different degrees of counterion association ϕ_1 and ϕ_2 coexist.



breaking and phase separation straightforward. When electrostatic interactions are present, the situation is less clear. First, any macroscopic phases that form interact electrostatically with each other, preventing the formation of a d -region with constant pressure and thus the application of the Maxwell construction. Second, macroscopic phases may not form in the first place because the electrostatic contribution to the line tension between coexisting phases is negative.⁴⁸ This may lead to modulated phase structures that are characterized by a certain length scale.⁵⁰ Modulated phases on different macroions may then correlate. Third, a term penalizing gradients in the degree of counterion association may be present in the free energy. If that penalty is sufficiently high, it will lead to different and yet homogeneous degrees of counterion association on each macroion. In this case, the present model will apply. To sum up, to systematically account for heterogeneous degrees of counterion association along each macroion would be an interesting subject but is beyond the scope of the present study.

6.6 Comparison with model proposed by Majee *et al.*³⁴

Majee *et al.*³⁴ previously studied two interacting planar macroions with a charge regulation model governed by the Frumkin–Fowler–Guggenheim isotherm. They employ the notation $\chi_M = 2\chi$ and $\lambda_M = \lambda - \chi$ in a free energy expression that is formally identical to eqn (2), yet with two differences. First, salt is present at a fixed chemical potential and corresponding Debye length l_D . Second, the number density of surface charges is $(1/2 - \phi)e/a$, in contrast to $(1 - \phi)e/a$ used in the present work. This choice introduces additional adsorption sites, allowing the surface charge density to change sign and enabling attractive interactions between macroions with asymmetric degrees of dissociation $\phi_1 \neq \phi_2$. Owing to the absence of simple analytic solutions of the Poisson–Boltzmann equation for interacting surfaces in the presence of salt and to the five-dimensional parameter space of the model, their study is restricted to selected examples that demonstrate symmetry breaking, without a systematic characterization of metastable regions, critical behavior, or the role of electrostatic interactions for the spontaneous symmetry breaking.

The consideration of the stability of an isolated planar macroion clearly illustrates the differences of the model proposed by Majee *et al.*³⁴ to our present work. Using our present notation, their free energy for a single planar isolated macroion reads

$$\frac{aF}{A} = f_{\text{BW}}(\phi) - \lambda\phi + 2\left(\frac{1}{2} - \phi\right) \left[\frac{1-q}{p} + \ln(p+q) \right], \quad (19)$$

with $p = (1/2 - \phi) \times l_D/(2B)$ and $q = \sqrt{p^2 + 1}$. Vanishing second derivative of aF/A with respect to ϕ yields a spinodal line

$$\chi = \frac{1}{2\phi(1-\phi)} + \frac{1}{\sqrt{(2B/l_D)^2 + \left(\frac{1}{2} - \phi\right)^2}} \quad (20)$$

that is different from eqn (17) and implies a critical point $\chi = 2$ at $\phi = 0.5$ in the large salt limit ($l_D \rightarrow 0$) and $\chi = 6.458$ at $\phi = 0.203$ in the no-salt limit ($l_D \rightarrow \infty$). Majee *et al.*³⁴ have explored non-ideality parameters up to $\chi = 20$ (that is, $\chi_M = 40$ for their definition of the non-ideality parameter), suggesting the isolated macroions would not necessarily be stable with respect to separating into different phases with distinct values of ϕ . For our present model we ensure isolated macroions are stable by choosing $\chi < 3.732$, as discussed in Section 6.4.

7 Conclusions

In this work we have analyzed a theoretical model for two interacting charge-regulated macroions, represented by two planar surfaces of the same bare charge density. The corresponding counterions can either be dissociated, thus residing in solution between the two macroions, or associated with the macroion surfaces through a Frumkin–Fowler–Guggenheim isotherm. This isotherm is structurally identical to the mean-field Bragg–Williams free energy of a lattice gas with interactions. That is, macroion charges that emerge from counterion dissociation are assumed to be subject of non-electrostatic interactions that can be attractive. No added salt is present.

We have shown that a spontaneous symmetry breaking can occur, leaving the two macroion surfaces with unequal degrees of dissociation and thus unequal effective charge densities. Analytic results show that, if present, symmetry breaking occurs only at intermediate distances between the two macroions, but not for sufficiently small or large distances. A three-dimensional stability diagram describes all parameter combinations where symmetry breaking is observed, either in the presence of metastable symmetric states or in their absence. Regions with metastable states do not exist near critical points.

We have discussed that our assumption of modeling the interaction between planar macroions in the complete absence of salt will become applicable if the Debye screening length $l_D \gg a/l_B$ is much larger than the typical cross-sectional area per charge a on the macroion divided by the Bjerrum length l_B . For example, $a = 10 \text{ nm}^2$ and $l_B = 1 \text{ nm}$ would require a salt concentration significantly smaller than 1 mM. Many experimental systems carried out at low salt content will satisfy the condition $l_D \gg a/l_B$. Another important assumption of our work is the uniformity of the degree of association/dissociation on each macroion. To ensure this is always the case at least for an isolated macroion, we have imposed the upper limit $\chi < 3.732$ on our non-ideality parameter χ . The occurrence and structure of non-uniformly distributed degrees of counterion association for interacting macroions with $\chi < 3.732$ remains an open question. Finally, we have studied the role of electrostatic interactions for the symmetry breaking. Interestingly, the hypothetical process of switching on the electrostatic interaction (that is, increasing the Bjerrum length l_B) reveals a tendency to stabilize the symmetric counterion association state $\phi_1 = \phi_2$. It is thus appropriate to state that, if present,



symmetry breaking occurs not because of electrostatic interactions but in spite of them.

The present work offers a comprehensive understanding of spontaneous symmetry breaking for planar macroions in the absence of salt, based on the Frumkin–Fowler–Guggenheim isotherm. It complements preceding case studies in the presence of salt and for non-planar geometries,^{34–37} where analytic results are not available.

Conflicts of interest

There are no conflicts to declare.

Data availability

All data that support the findings of this study are included within the article.

Acknowledgements

G. V. B. thanks Fondecyt (grant no. 11240064) for support.

Notes and references

- G. Gonella, E. H. G. Backus, Y. Nagata, D. J. Bonthuis, P. Loche, A. Schlaich, R. R. Netz, A. Kühnle, I. T. McCrum and M. T. M. Koper, *et al.*, *Nat. Rev. Chem.*, 2021, **5**, 466–485.
- I. Popa, P. Sinha, M. Finessi, P. Maroni, G. Papastavrou and M. Borkovec, *Phys. Rev. Lett.*, 2010, **104**, 228301.
- A. Kubincová, P. H. Hünenberger and M. Krishnan, *J. Chem. Phys.*, 2020, **152**, 104713.
- S. Wang, R. Walker-Gibbons, B. Watkins, M. Flynn and M. Krishnan, *Nat. Nanotechnol.*, 2024, **19**, 485–493.
- S. Wang, R. Walker-Gibbons, B. Watkins, B. Lin and M. Krishnan, *Nat. Commun.*, 2025, **16**, 1–16.
- J. C. Neu, *Phys. Rev. Lett.*, 1999, **82**, 1072.
- A. Behjatian, R. Walker-Gibbons, A. A. Schekochihin and M. Krishnan, *Langmuir*, 2022, **38**, 786–800.
- J. E. Hallett, D. A. J. Gillespie, R. M. Richardson and P. Bartlett, *Soft Matter*, 2018, **14**, 331–343.
- Y. Avni, D. Andelman and R. Podgornik, *Curr. Opin. Electrochem.*, 2019, **13**, 70–77.
- T. Markovich, D. Andelman and R. Podgornik, *Europhys. Lett.*, 2018, **120**, 26001.
- A. Behjatian, R. Blossey and M. Krishnan, *J. Chem. Phys.*, 2025, **162**, 064901.
- S. H. Behrens and M. Borkovec, *Phys. Rev. E:Stat. Phys., Plasmas, Fluids, Relat. Interdiscip. Top.*, 1999, **60**, 7040.
- R. Pericet-Camara, G. Papastavrou, S. H. Behrens and M. Borkovec, *J. Phys. Chem. B*, 2004, **108**, 19467–19475.
- A. Bakhshandeh, D. Frydel, A. Diehl and Y. Levin, *Phys. Rev. Lett.*, 2019, **123**, 208004.
- D. Frydel, *J. Chem. Phys.*, 2019, **150**, 194901.
- A. Bakhshandeh, D. Frydel and Y. Levin, *Phys. Chem. Chem. Phys.*, 2020, **22**, 24712–24728.
- T. Curk and E. Luijten, *Phys. Rev. Lett.*, 2021, **126**, 138003.
- D. Izzo, A. Bakhshandeh and Y. Levin, *J. Chem. Phys.*, 2025, **163**, 064703.
- G. Trefalt, S. H. Behrens and M. Borkovec, *Langmuir*, 2016, **32**, 380–400.
- K. H. Chu and B. C. Tan, *Colloid Interface Sci. Commun.*, 2021, **45**, 100519.
- H. Tamura and R. Furuichi, *J. Colloid Interface Sci.*, 1997, **195**, 241–249.
- C. A. Başar, *J. Hazard. Mater.*, 2006, **135**, 232–241.
- K. Y. Foo and B. H. Hameed, *Chem. Eng. J.*, 2010, **156**, 2–10.
- W. Rudzinski and D. H. Everett, *Adsorption of gases on heterogeneous surfaces*, Academic Press, 2012.
- V. Kalinin and C. Radke, *Colloids Surf., A*, 1996, **114**, 337–350.
- V. Kolev, K. Danov, P. Kralchevsky, G. Broze and A. Mehreteab, *Langmuir*, 2002, **18**, 9106–9109.
- M. Volkova-Gugeshashvili, A. Volkov and V. Markin, *Russ. J. Electrochem.*, 2006, **42**, 1073–1078.
- N. S. Mousavi, A. Javadi, V. I. Kovalchuk, E. V. Aksenenko, G. Loglio, D. Vollhardt, E. Schneck and R. Miller, *Z. Phys. Chem.*, 2025, **239**, 1705–1724.
- A. Fomkin, A. Pribylov, I. Men'shchikov, A. Shkolin, O. Aksyutin, A. Ishkov, K. Romanov and E. Khozina, *Reactions*, 2021, **2**, 209–226.
- M. Levi and D. Aurbach, *Electrochim. Acta*, 1999, **45**, 167–185.
- S. A. Onaizi, M. Nasser and N. M. Al-Lagtah, *J. Surfactants Deterg.*, 2016, **19**, 645–652.
- H. Tamura, N. Katayama and R. Furuichi, *Environ. Sci. Technol.*, 1996, **30**, 1198–1204.
- S. J. Brugman, B. L. Werkhoven, E. R. Townsend, P. Accordini, R. van Roij and E. Vlieg, *J. Colloid Interface Sci.*, 2020, **559**, 291–303.
- A. Majee, M. Bier and R. Podgornik, *Soft Matter*, 2018, **14**, 985–991.
- A. Majee, M. Bier, R. Blossey and R. Podgornik, *Phys. Rev. Res.*, 2020, **2**, 043417.
- P. Khunpetch, A. Majee and R. Podgornik, *Soft Matter*, 2022, **18**, 2597–2610.
- H. Ruixuan, A. Majee, J. Dobnikar and R. Podgornik, *Eur. Phys. J. E:Soft Matter Biol. Phys.*, 2023, **46**, 115.
- H. T. Davis, *Statistical Mechanics of Phases, Interfaces, and Thin Films*, Wiley-VCH, New York, 1996.
- J. N. Israelachvili, *Intermolecular and Surface Forces*, Academic Press, London, 3rd edn, 2011.
- D. Andelman, *Handbook of biological physics*, Elsevier, 1995, vol. 1, pp. 603–642.
- C. J. Van Oss, M. K. Chaudhury and R. J. Good, *Chem. Rev.*, 1988, **88**, 927–941.
- S. H. Behrens and D. G. Grier, *J. Chem. Phys.*, 2001, **115**, 6716–6721.
- H. E. Bergna and W. O. Roberts, *Colloidal silica: fundamentals and applications*, CRC Press, 2005.
- S. Oversteegen and H. Lekkerkerker, *Phys. Rev. E:Stat., Nonlinear, Soft Matter Phys.*, 2003, **68**, 021404.



- 45 S. May, D. Harries and A. Ben-Shaul, *Phys. Rev. Lett.*, 2002, **89**, 268102.
- 46 C. L. Baciú and S. May, *J. Phys.:Condens. Matter*, 2004, **16**, S2455.
- 47 W. M. Gelbart and R. Bruinsma, *Phys. Rev. E:Stat. Phys., Plasmas, Fluids, Relat. Interdiscip. Top.*, 1997, **55**, 831.
- 48 G. V. Bossa, M. A. Brown, K. Bohinc and S. May, *Int. J. Adv. Eng. Sci. Appl. Math.*, 2016, **8**, 101–110.
- 49 G. B. Arfken, H. J. Weber and F. E. Harris, *Mathematical methods for physicists: a comprehensive guide*, Academic Press, 2011.
- 50 D. Andelman and R. E. Rosensweig, *J. Phys. Chem. B*, 2009, **113**, 3785–3798.

